Pergamon

0301-9322(95)00063-1

Int. J. Multiphase Flow Vol. 22, No. 1, pp. 185–194, 1996

0301-9322/96 $15.00 + 0.00

STOKES FLOW THROUGH AN ARRAY OF RECTANGULAR FIBERS

C. Y. WANG

Departments of Mathematics and Mechanical Engineering, Michigan State University, East Lansing, MI 48824, U.S.A.

(Received 8 February 1995; in revised form 2 August 1995)

Abstract—The slow viscous flow through an array of rectangular fibers is solved by the efficient method of eigenfunction expansion and domain decomposition. In particular, the normalized permeability is determined for square fibers and strips in rectangular arrays. The limitations of the approximate capillary model and the obstacle model are shown. An empirical formula for the drag of a single square fiber is also given.

Key Words: porous medium, permeability, Stokes flow

INTRODUCTION

The study of the flow through porous media is important in numerous biological and engineering processes. Usually, satisfactory predictions can be obtained by Darcy's law which treats the medium as a continuum. However, the necessary macroscopic parameters, such as permeability, can only be theoretically predicted through microscopic analysis of the fluid path through the pores of the solid matrix. In this respect, two distinct approaches seem to have emerged. The first approach models the pores of a porous medium as a bunch of capillary tubes which may be tortuous or interconnected in a network. Essentially, the resistance to flow is through Poiseuille drag in a tube. The second approach considers the solid matrix as a cluster of immobile solid obstacles, which contribute a collective Stokes resistance to the flow. For a review of these theories one may consult Scheidegger (1974), Dagan (1989), Adler (1992) and Dullien (1992).

It is evident that the capillary models would best describe pores and crevices which are indeed long and slender, while the obstacle models would be better suited for porous media with large void fractions. It is, therefore, advisable to rigorously study a class of matrix geometries which could link both capillary and obstacle extremes and thus quantify the limits of their applicabilities.

The most rigorous microscopic analyses solve the Stokes equations for creeping flow between periodic bodies. The existing literature considers a porous medium only consisting of arrays of solid spheres or cylinders (Hasimoto 1959; Sangani & Acrivos 1982; Zick & Homsy 1982; Drummond & Tahir 1984). When the solids are dilute, the geometry may represent the obstacle approach. However, small capillary channels cannot be formed with spheres and cylinders even when they are closely packed.

In this paper, we shall solve the Stokes flow across an array of rectangular cylinders. This particular geometry has the advantage of being able to represent both the capillary and the obstacle extremes. A practical application for rectangular fibers is in the modeling of rock fissures (Dagan 1989).

FORMULATION

Figure 1(a) shows a porous medium composed of a doubly periodic array of rectangular fibers. If the geometric ratios a, b and c are such that $a \gg 1$, $b \gg 1$ and $c = 0(1)$, then a network of channels exists and the capillary approach may be useful. If $a \ll 1$, $0 < b - 1 \ll 1$ and $c = 0(1)$, then the fibers are dilute and the obstacle approach may apply. However, if a, b and c are all order of unity as

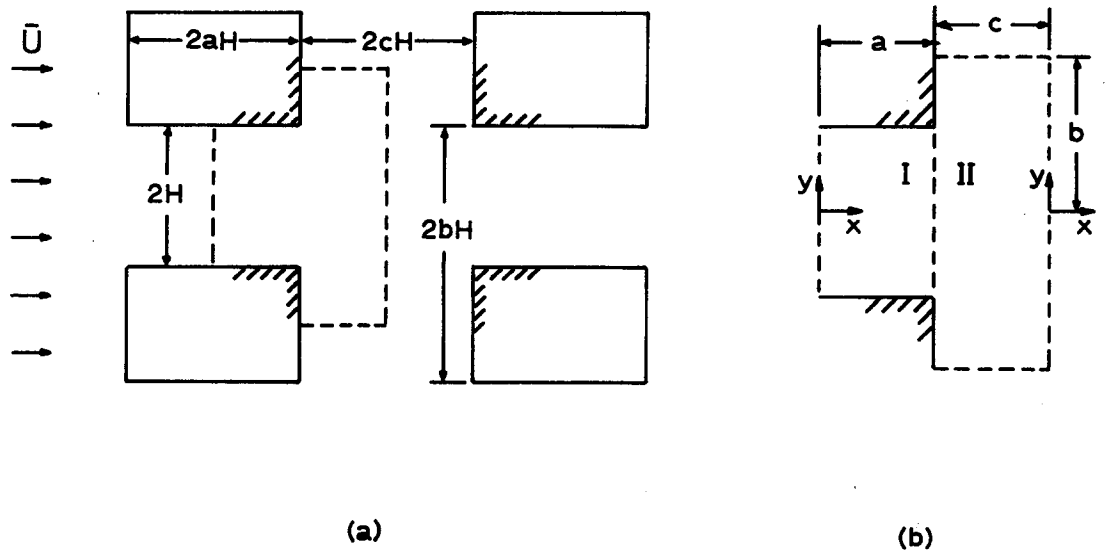

Figure 1. (a) Geometry and (b) partition into two regions.

shown, neither approach is valid, and the rsistance must be obtained by solving the Stokes equation.

We assume a fluid of viscosity μ is forced from the left, parallel to one of the axes of the rectangle, with an average macroscopic velocity $\bar{U} = U/b$. Then, the mass flux (per depth) through each horizontal pore is $2UH$. The Strokes equation is

$$p_x = (\nabla^2\psi)_y, \tag{1}$$

$$p_y = -(\nabla^2\psi)_x, \tag{2}$$

where p is the pressure normalized by $\mu U/H$, ψ is the stream function normalized by UH and x and y are Cartesian coordinates normalized by H. The stream function satisfies the biharmonic

$$\nabla^4\psi = 0. \tag{3}$$

The boundary conditions are that on the solid rectangles, the stream function is constant (± 1) and that the normal derivative of ψ is zero. Our aim is to find the pressure drop or premeability to this forced flow.

Previous literature which studied cylindrical or spherical inclusions used an expansion in cylindrical or spherical harmonics, which is inapplicable in the present case. We shall use an eigenfunction expansion and matching method, probably first used by Weil (1951) and extended by Dagan *et al.* (1982) and Wang (1993). In essence, the fluid domain is partitioned into simple regions, solved separately by eigenfunctions and matched along their common boundary.

Due to symmetry, we need to consider only the T-shaped domain in figure 1(a). Figure 1(b) shows the partition of the domain into two regions, I and II, each with their respective Cartesian axes at their respective symmetry points. The boundary conditions for $\psi_{\rm I}(x, y)$ are

$$\psi_{\rm I}(x, \pm 1) = \pm 1, \tag{4}$$

$$\psi_{{\rm I}_y}(x, \pm 1) = 0, \tag{5}$$

$$\psi_{{\rm I}_x}(0, y) = 0, \quad \psi_{{\rm I}_{xxx}}(0, y) = 0 \tag{6}$$

The boundary conditions for $\psi_{\rm II}(x, y)$ are

$$\psi_{\rm II}(x, \pm b) = \pm 1, \tag{7}$$

$$\psi_{{\rm II}_{yy}}(x, \pm b) = 0, \tag{8}$$

$$\psi_{{\rm II}_x}(0, y) = 0, \quad \psi_{{\rm II}_{xxx}}(0, y) = 0, \tag{9}$$

$$\psi_{II}(-c, y) = \text{sign}(y), \quad 1 < |y| < b, \tag{10}$$

$$\psi_{II_x}(-c, y) = 0, \quad 1 < |y| < b. \tag{11}$$

Furthermore, ψ_I and ψ_{II} match continuously at their common boundary

$$\psi_{II}(-c, y) = \psi_I(a, y), \quad |y| < 1, \tag{12}$$

$$\psi_{II_x}(-c, y) = \psi_{I_x}(a, y), \quad |y| < 1, \tag{13}$$

$$\psi_{II_{xx}}(-c, y) = \psi_{I_{xx}}(a, y), \quad |y| < 1, \tag{14}$$

$$\psi_{II_{xxx}}(-c, y) = \psi_{I_{xxx}}(a, y), \quad |y| < 1. \tag{15}$$

EIGENFUNCTION EXPANSIONS

The general solution of ψ_I satisfying [3], [4] and [6] is

$$\psi_I = \sum_{n=1}^{\infty} [A_n Q_n(x) + B_n R_n(x)] \sin \alpha_n y + \sum_{n=1}^{\infty} C_n S_n(y) \cos \beta_n x + C_0(y - y^3) + \tfrac{1}{2}(3y - y^3), \tag{16}$$

where $\alpha_n = n\pi$, $\beta_n = n\pi/a$ and

$$Q_n(x) = e^{\alpha_n(x-a)} + e^{-\alpha_n(x+a)}, \tag{17}$$

$$R_n(x) = x(e^{\alpha_n(x-a)} - e^{-\alpha_n(x+a)}), \tag{18}$$

$$S_n(y) = e^{\beta_n(y-1)} - e^{-\beta_n(y+1)} - \left(\frac{1 - e^{-2\beta_n}}{1 + e^{-2\beta_n}}\right) y(e^{\beta_n(y-1)} + \beta^{-\beta_n(y+1)}). \tag{19}$$

Equation [5] is equivalent to

$$\sum_{n=1}^{\infty} [A_n Q_n(x) + B_n R_n(x)] \alpha_n (-1)^n + \sum_{n=1}^{\infty} C_n S_n'(1) \cos \beta_n x - 2C_0 = 0. \tag{20}$$

Thus, the coefficients C_n can be found by Fourier inversion of [20]

$$C_0 = \frac{1}{2a} \sum_{m=1}^{\infty} (-1)^m \left\{ A_m(1 - e^{-2a\alpha_m}) + B_m \left[\left(a + \frac{1}{m\pi} \right) e^{-2a\alpha_m} - \frac{1}{m\pi} + a \right] \right\}, \tag{21}$$

$$C_n = -\frac{2\pi}{aS_n'(1)} \sum_{m=1}^{\infty} (A_m Q_{1mn} + Q_{1mn} + B_m R_{1mn}) m(-1)^m, \tag{22}$$

where

$$Q_{1mn} = \int_0^a Q_m \cos \beta_n x \, dx = \frac{(-1)^n m a^2}{\pi(a^2 m^2 + n^2)} (1 - e^{-2am\pi}), \tag{23}$$

$$R_{1mn} = \int_0^a R_m \cos \beta_n x \, dx = \frac{(-1)^n a^2}{\pi(a^2 m^2 + n^2)} [(a^2 m^2 - n^2 + a^3 m^3 \pi + amn^2 \pi) e^{-2am\pi} + n^2 - a^2 m^2 + a^3 m^3 \pi + amn^2 \pi]. \tag{24}$$

The form of [16] is complete since ψ_I is left with two independent series solutions represented by A_n and B_n on the fourth boundary at $x = a$. The form of ψ_{II} is similar, but somewhat different:

$$\psi_{II}(x, y) = \sum_{n=1}^{\infty} [D_n T_n(x) + E_n U_n(x)] \sin \gamma_n y + y/b, \tag{25}$$

where $\gamma_n = \pi/b$ and

$$T_n(x) = e^{\gamma_n(x-c)} + e^{-\gamma_n(x+c)}, \tag{26}$$

$$U_n(x) = x(e^{\gamma_n(x-c)} - e^{\gamma_n(x+c)}). \tag{27}$$

Equation [25] satisfies [5], [7], [8] and [9]. Next, we multiply [10] and [12] by $\sin \gamma_n y$ and integrate from $y = 0$ to $y = b$.

$$\frac{b}{2}[D_n T_n(-c) + E_n U_n(-c)] + \frac{1}{b}\int_0^b y \sin \gamma_n y \, dy = \int_1^b \sin \gamma_n y \, dy + \sum_{m=1}^{\infty} [A_m Q_m(a) + B_m R_m(a)] I_{nm} + \sum_{m=1}^{\infty} C_m (-1)^m J_{mn} + c_0 \int_0^1 (y - y^3)\sin \gamma_n y \, dy + \frac{1}{2}\int_0^1 (3y - y^3) \sin \gamma_n y \, dy, \quad [28]$$

where

$$I_{nm} = \int_0^1 \sin \alpha_m y \sin \gamma_n y \, dy = \begin{cases} \dfrac{b^2 m(-1)^m \sin \gamma_n}{\pi(n^2 - b^2 m^2)} & n \neq bm \\ \dfrac{1}{2} & n = bm \end{cases}, \quad [29]$$

$$J_{mn} = \int_0^1 S_m(y)\sin \gamma_n y \, dy = \{-2a^3 b^3 mn(1 - e^{-2\beta_m})^2 \cos \gamma_n + ab^2 \sin \gamma_n [a(a^2 n^2 - b^2 m^2)e^{-4\beta_m} + 4m\pi(b^2 m^2 + a^2 n^2)e^{-2\beta_m} + a(b^2 m^2 - a^2 n^2)]\}/[(1 + e^{-2\beta_m})(b^2 m^2 + a^2 n^2)^2 \pi^2]. \quad [30]$$

Equation [28] is simplified to

$$\frac{b}{2}[D_n(1 + e^{-2c\gamma_n}) + cE_n(1 - e^{-2c\gamma_n})] = \sum_{m=1}^{\infty} [A_m Q_m(a) + B_m R_m(a)] I_{nm} + \sum_{m=1}^{\infty} C_m (-1)^m J_{mn} - 2C_0[3\gamma_n \cos \gamma_n + (\gamma_n^2 - 3)\sin \gamma_n]/\gamma_n^4 + 3(\sin \gamma_n - \gamma_n \cos \gamma_n)/\gamma_n^4. \quad [31]$$

Similarly, [11] and [13] are inverted

$$\frac{b}{2}\{D_n \gamma_n(e^{-2c\gamma_n} - 1) + E_n[e^{-2c\gamma_n} - 1 - c\gamma_n(1 + e^{-2c\gamma_n})]\} = \sum_{m=1}^{\infty} [A_m Q'_m(a) + B_m R'_m(a)] I_{nm}. \quad [32]$$

Now [14] is multiplied by $\sin \alpha_n y$ and integrated from $y = 0$ to $y = 1$. The result is

$$\sum_{m=1}^{\infty} \{D_m \gamma_m^2(1 + e^{-2c\gamma_m}) + E_m[2\gamma_m(1 + e^{-2c\gamma_m}) + c\gamma_m^2(1 - e^{-c\gamma_m})]\} I_{mn} = \tfrac{1}{2}[A_n Q''_n(a) + B_n R''_n(a)] - \sum_{m=1}^{\infty} C_m \beta_m^2 (-1)^m K_{mn}. \quad [33]$$

Note that I_{mn} is the transpose of I_{nm} and

$$K_{mn} = [-2a^3 mn(1 - e^{-2\beta_n})^2(-1)^n]/[(1 + e^{-2\beta_m})(m^2 + a^2 n^2)^2 \pi^2]. \quad [34]$$

Lastly, [15] is inverted

$$\sum_{m=1}^{\infty} \{D_m \gamma_m^3(e^{-2c\gamma_m} - 1) + E_m[3\gamma_m(e^{-2c\gamma_m} - 1) - c\gamma_m^3(1 + e^{-c\gamma_m})]\} I_{mn} = \tfrac{1}{2}[A_n Q'''_n(a) + B_n R'''_n(a)]. \quad [35]$$

Equations [22], [31]–[33] and [35] represent five sets of equations and five sets of unknowns: A_n, B_n, C_n, D_n and E_n. The problem is, in principle, solved. We truncate D_n and E_n to N terms and, due to a shorter width, A_n, B_n, C_n to $M =$ integer (N/b) terms. Together with C_0, there are $2N + 3M + 1$ equations and unknowns. The error is decreased by increasing N normally $N \sim 10$ gives 1% error. Since Fourier series is absolutely and uniformly convergent, and Stokes flow is highly diffusive, convergence is very fast.

THE PRESSURE DISTRIBUTION

After the stream function is determined, one can solve for the pressure from [1] and [2]

$$p_{\mathrm{I}}(x,y)=\sum_{n=1}^{\infty}B_n 2\alpha_n(e^{\alpha_n(x-a)}-e^{-\alpha_n(x+a)})\cos a_n y-\sum_{n=1}^{\infty}2\beta_n C_n\left(\frac{1-e^{-2\beta_n}}{1+e^{-2\beta_n}}\right)\cdot$$
$$\times(e^{\beta_n(y-1)}+e^{-\beta_n(y+1)})\sin\beta_n x-(6C_0+3)x+p_0, \quad [36]$$

$$p_{\mathrm{II}}(x,y)=\sum_{n=1}^{\infty}E_n 2\gamma_n(e^{\gamma_n(x-c)}-e^{-\gamma_n(x+c)})\cos\gamma_n y+p_1. \quad [37]$$

Here p_0 and p_1 are the pressures at the two coordinate origins. Matching the pressures at the boundary yields

$$p_{\mathrm{I}}(a,y)=p_{\mathrm{II}}(-c,y). \quad [38]$$

Integrating [38] from $y=0$ to $y=1$ gives

$$-3a(2C_0+1)+p_0=\sum_{n=1}^{\infty}E_n 2(e^{-2c\gamma_n}-1)\sin\gamma_n+p_1. \quad [39]$$

The mean pressure drop per unit distance is thus

$$G=\frac{\Delta p}{\Delta x}=\frac{(p_0-p_1)}{(a+c)}=\frac{1}{(a+c)}\left[\sum_{n=1}^{\infty}E_n(e^{-2c\gamma_n}-1)\sin\gamma_n+3a(2C_0+1)\right]. \quad [40]$$

Since the average velocity is U/b, Darcy's law is

$$\bar{U}=\frac{U}{b}=\frac{K}{\mu}\frac{\Delta p}{\Delta x}\frac{\mu U}{H^2}, \quad [41]$$

where K is the permeability. The normalized permeability is thus

$$\frac{K}{H^2}=\frac{1}{bG}, \quad [42]$$

where G is from [40].

SOME APPROXIMATIONS

If $a\gg 1$, we may assume almost all resistance is due to Poiseuille flow through the narrow horizontal channels. This is the capillary approach. The normalized pressure drop through a channel of width $2H$ and length aH is $3a$. The pressure drop per period is $3a/(a+c)$. Thus, the equivalent permeability is

$$\frac{K}{H^2}=\frac{a+c}{3ab}. \quad [43]$$

On the other hand, if $a\to 0$ and $c\gg 1$, the solid matrix can be regarded as a series of vertical screens. The case for a single vertical screen with zero thickness ($a=0, c=\infty$) was solved analytically by Hasimoto (1958). He found the conductance (in our variables) of one slit is

$$\frac{\text{flow}}{\text{pressure drop}}=\frac{b^2H^2}{\pi\mu}\left|\ln\cos\left(\frac{\pi}{2b}\right)\right|. \quad [44]$$

Thus, for a series of screens spaced $2cH$ apart, the permeability is

$$\frac{K}{H^2}=\frac{cb}{\pi}\left|\ln\cos\left(\frac{\pi}{2b}\right)\right|. \quad [45]$$

If $a\ll 1$, $0<b-1\ll 1$, $c\geqslant 0(1)$, the solid fibers are sparsely distributed, and the obstacle approach may be considered. For a circular cylinder, various analytical approximations using

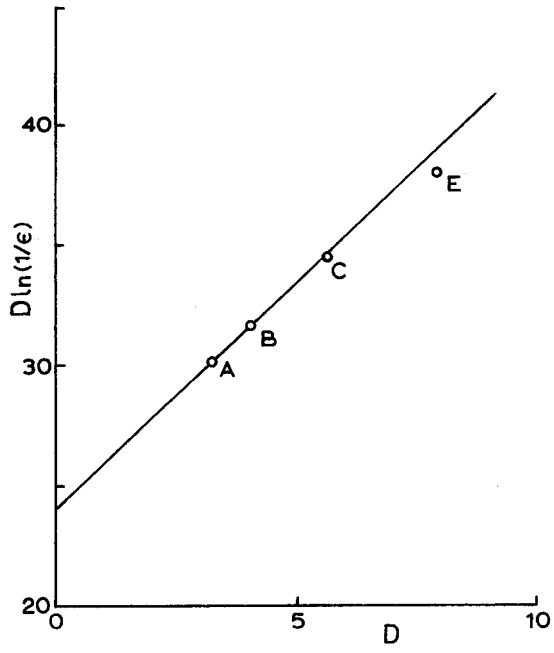

Figure 2. Extrapolation to the flow across a single square clinder A: $a = 0.01$, $\epsilon = 0.00098$; B: $a = 0.02$, $\epsilon = 0.00038$; C: $a = 0.05$, $\epsilon = 0.00227$; and E: $a = 0.1$, $\epsilon = 0.00826$.

cylindrical harmonics by Hasimoto (1959), Happel (1959) and Kuwabara (1959) yield the drag on a single cylinder in the form

$$\frac{F}{\mu U} = \frac{4\pi}{\frac{1}{2}\ln\left(\frac{1}{\epsilon}\right) - \delta_1}. \qquad [46]$$

Here, F is the drag per unit length of a cylinder, ϵ is the solid fraction and δ_1 is a constant, depending on the model, varying between 0.5 and 0.75. For the rectangular cylinders studied here, similar analyses do not exist. However, an empirical law similar to [46] can be obtained by extrapolation. We shall illustrate using square cylinders.

Considering a square cell enclosing the square cylinder ($a = b - 1$) with equal gap width ($c = 1$), the solid fraction is (a^2/b^2). Similar to [46], the non-dimensional drag is written as

$$D \equiv \frac{F}{\mu U} = \frac{\kappa}{\ln\left(\frac{1}{\epsilon}\right) - \delta}. \qquad [47]$$

The constants κ and δ are to be determined as $\epsilon = a^2(a+1)^{-2} \to 0$. For a given a, the factor D is computed from our series solution

$$D = 4b^2(p_0 - p_1). \qquad [48]$$

We rewrite [47] as

$$D \ln\left(\frac{1}{\epsilon}\right) = \kappa + D\delta. \qquad [49]$$

Then, $D \ln(1/\epsilon)$ is plotted against D in figure 2. In order to increase accuracy, up to 50 terms are retained in [40]. Extrapolating to $D = 0$, we find $\kappa = 24.0$ and $\delta = 1.89$. Using [47], the permeability for sparsely-spaced square cylinders can be approximated by

$$\frac{K}{H^2} = \frac{(a+1)(a+c)}{6.0}\left[2 \ln\left(1 + \frac{1}{a}\right) - 1.89\right]. \qquad [50]$$

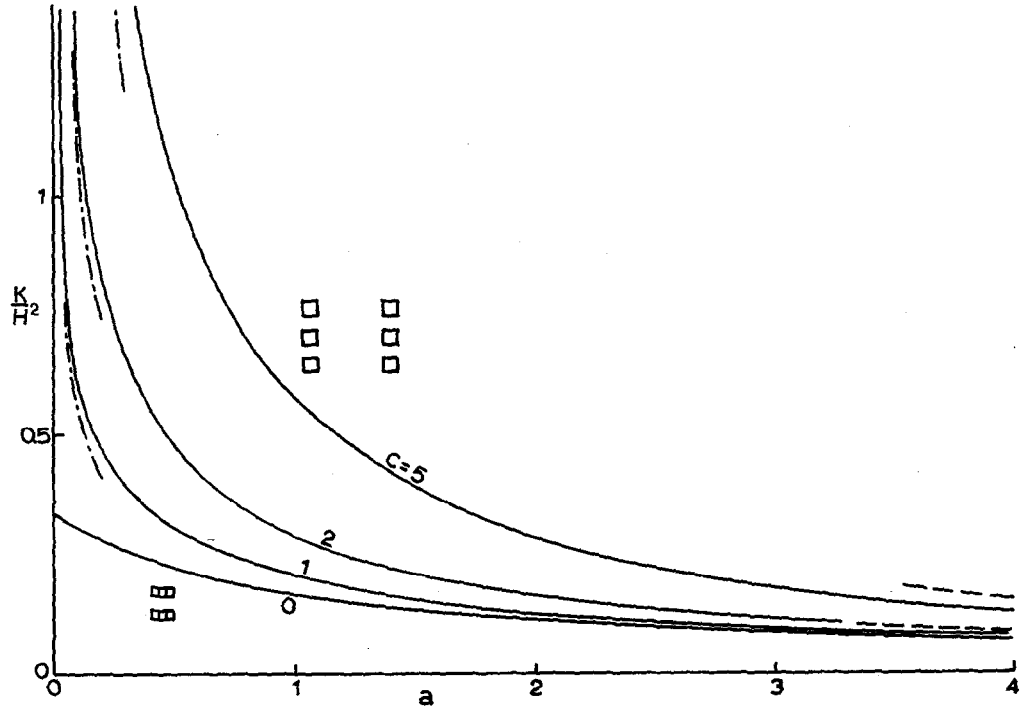

Figure 3. Permeability of square fibers in a rectangular array. ---, [43]; - - - - -, [50].

The limits of validity of this formula will be determined by comparison with the exact computation in the next section.

RESULTS AND DISCUSSION

The extreme cases $a \gg 1$ and $a \ll 1$ have been discussed in the previous section. For $a = 0(1)$ no analytical formulae exist. However, we have successfully computed permeability using

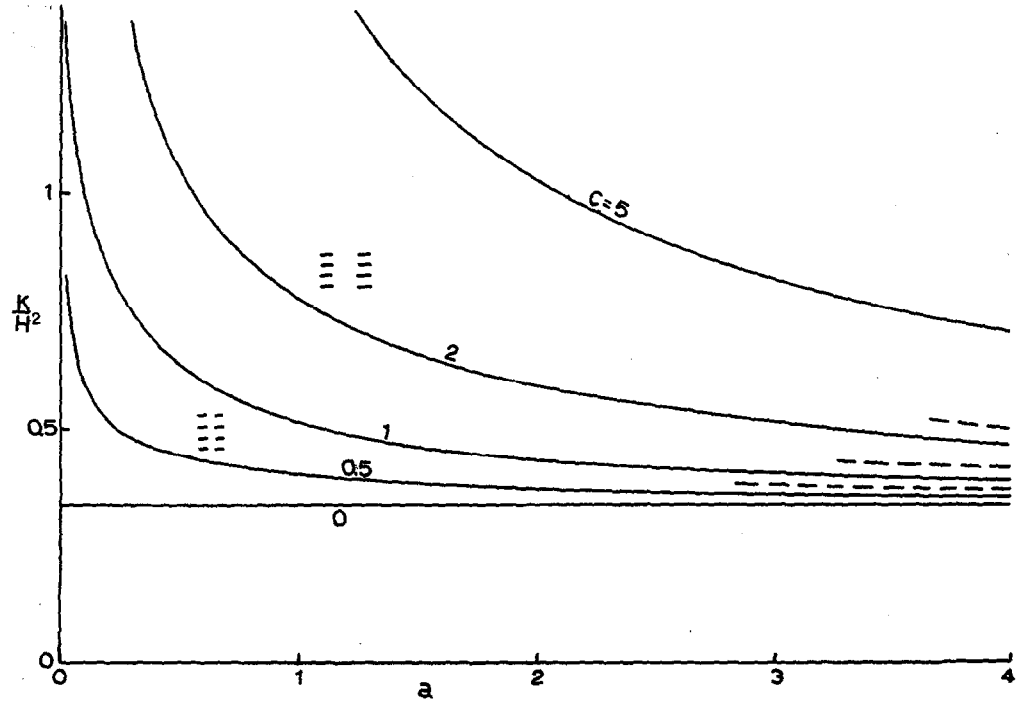

Figure 4. Permeability for an array of strips parallel to flow. ---, [43].

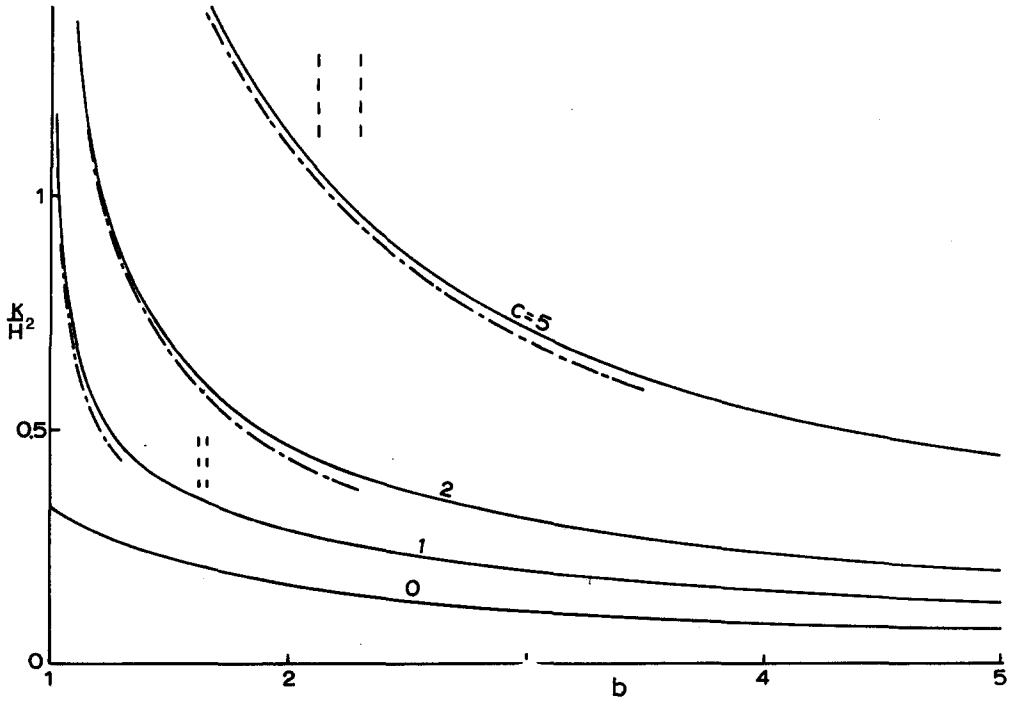

Figure 5. Permeability for an array of strips perpendicular to flow. – – – –, [45].

eigenfunction expansions introduced earlier. The results for $a = 0(1)$ are presented in the following discussion.

Our results shall be presented in terms of normalized permeability K/H^2, which is more useful than the normalized force per length D. The relation is $D = 4b(a + c)/(K/H^2)$. Also, we shall use the geometric ratios a, b and c instead of volume fraction as independent variables, since for zero thickness strips, the solid fraction, always being zero, ceases to be an index. Figure 3 shows the permeability for square fibers ($a = b - 1$) and various constant c. For $c = 0$, the fibers are horizontally stacked such that infinite parallel channels conduct the flow with permeability $1/3(a + 1)$. For $a > c$, the difference in permeability is small, showing the vertical channels have little effect. But, for $c > a$, the permeability is greatly increased. Also shown in figure 3 are the asymptotic approximations [43] and [50]. It is seen that the capillary model, which ignores entrance and exit effects, is valid only for channels whose length is at least five times its width, while the

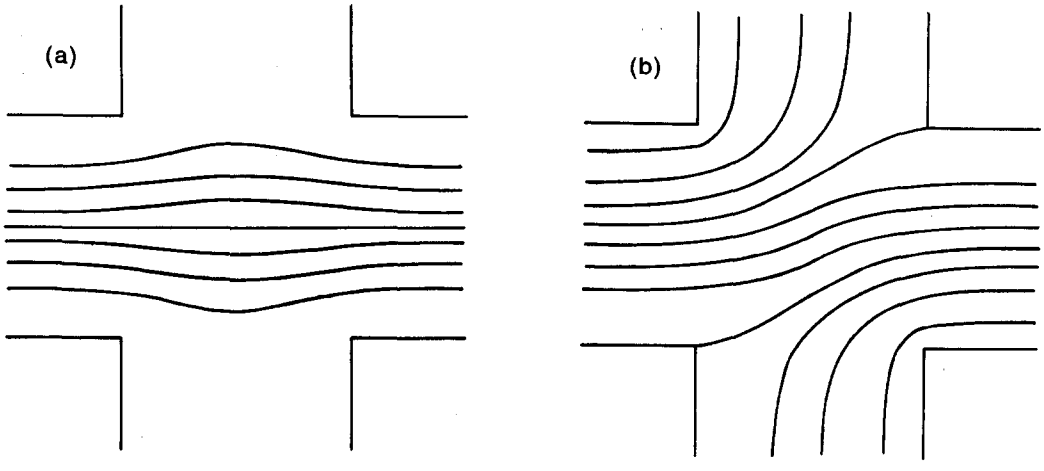

Figure 6(a) and (b). *Caption opposite.*

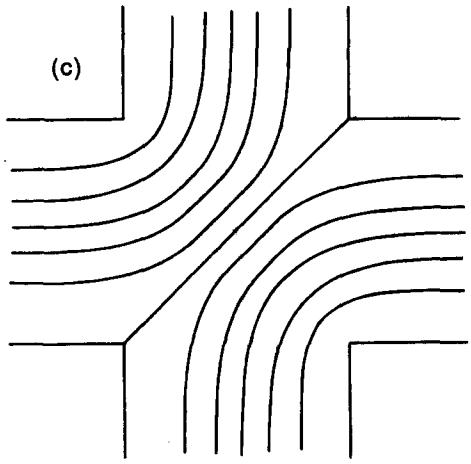

Figure 6(c)

Figure 6. Streamlines past square fibers ($a = c = 1$, $b = 2$). (a) Mean velocity horizontal, (b) mean velocity tilted 22.5° and (c) mean velocity tilted 45°.

obstacle model, if applicable, is valid for fiber sizes at most 0.1 of distance to its nearest neighbors. Figure 4 shows the permeability for horizontal (zero-thickness) strips ($b = 1$). When $c = 0$, we have parallel channels with $K/H^2 = 1/3$. The case of the vertical stips ($a = 0$) is shown in figure 5. Again, when $c = 0$, the strips are horizontally stacked into channels ($K/H^2 = 1/3b$). Our approximation [45], modified from Hasimoto's (1958) single screen result, becomes more applicable for large c. Results for rectangular fiber of other aspect ratios are similar and will not be presented here.

Anisotropy is evident from figures 4 and 5. The geometry $a = 0$, $b = 2$, $c = 1$, if turned 90°, is

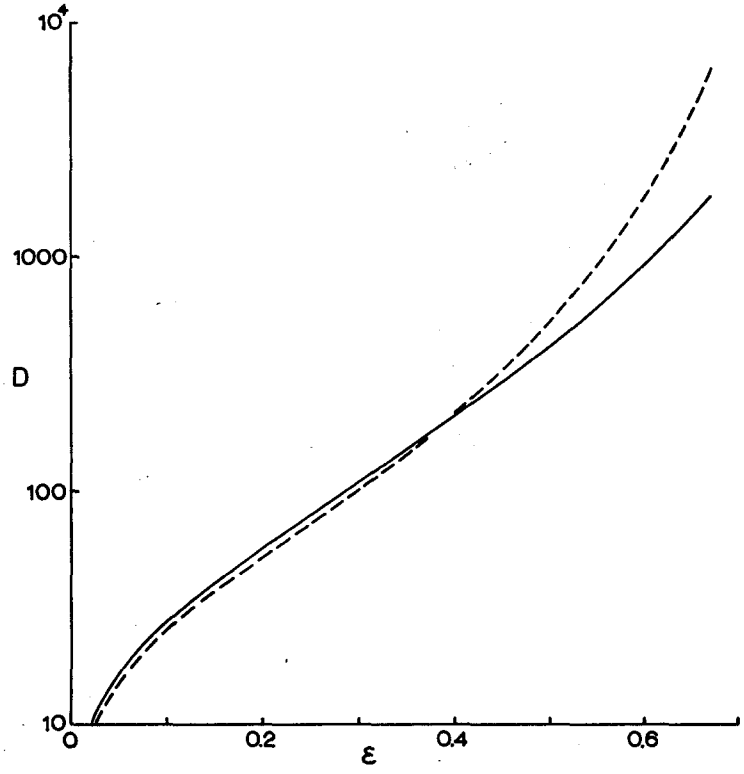

Figure 7. Normalized drag D as a function of solid fraction ϵ. Solid lines are square fibers in a square array (from figure 3), dashed lines are circular fibers in a square array (from Sangani & Acrivos 1982).

the same as that of $a = 1$, $b = 1$, $c = 1$. We find that the permeability of flow parallel to the strips is much higher than that normal to the strips. In a coordinate system coinciding with the principle axes of an orthotropic material, the permeability tensor is diagonalized to the values shown in our figures (Scheidegger 1974).

Our method also yields detailed streamlines. Figure 6(a) shows the horizontal flow through square fibers in a square array ($a = 1 = c, b = 2$). The flow in the vertical channels is almost stagnant. By superposition, one can obtain flows not parallel to the principle axes of the solid matrix. Figure 6(b) shows the result for the same mean velocity, but tilted 22.5°; while figure 6(c) shows the stramlines if velocity is tilted 45°. The detailed flow fields are necessary for the prediction of transport properties.

Figure 7 shows a comparison between square arrays of circular and square fibers. For low solid fraction ϵ (less than about 0.39), the circular fibers have slightly less drag (8% less) probably due to its more rounded shape. For high solid fractions the circular fibers have much larger drag due to obstruction of the passages. In fact, circular fiber drag becomes infinity as $\epsilon \to \pi^2/4 = 0.7854$ while the square fiber drag would not become infinity until $\epsilon \to 1$.

Since Stokes flow is linear, the assumption of zero Reynolds number necessarily leads to Darcy's law (see, for example, Scheidegger 1974). The condition for low Reynolds number is $\rho \bar{U} bH/\mu \ll 1$ where ρ is the density and $2bH$ is the transverse period. Notice, as in channel flow, the height of each stream tube is fixed and the streamwise parameters a, c do not alter the order of magnitude of the inertial effects.

By using the method of eigenfunction expansions and matching contiguous regions, we are successful in solving the Stokes flow through an array of rectangular fibers. The method is as efficient as using boundary integrals and is superior to using finite differences. Our permeability results should be quite useful in the prediction of the Darcy constant for porous media.

Acknowledgement—This research was partially supported by NIH Grant RR 01243.

REFERENCES

Adler P. M. 1992 *Porous Media, Geometry and Transports*. Butterworth–Heinemann, Boston, MA.

Dagan, G. 1989 *Flow and Transport in Porous Formations*. Springer, Berlin.

Dagan, Z., Weinbaum, S. & Pfeffer, R. 1982 An infinite-series solution for the creeping motion through an orifice of finite length. *J. Fluid Mech.* **115,** 505–523.

Drummond, J. E. & Tahir, M. I. 1984 Laminar viscous flow through arrays of parallel solid cylinders. *Int. J. Multiphase Flow* **10,** 515–540.

Dullien, F. A. L. 1992 *Porous Media–Fluid Transport and Pore Structure*, 2nd edn. Academic Press, San Diego, CA.

Happel, J. 1959 Viscous flow relative to arrays of cylinders. *AIChE Jl* **5,** 174–177.

Hasimoto, H. 1958 On the flow of a viscous fluid past a thin screen at small Reynolds numbers. *J. Phys. Soc. Jap.* **13,** 633–639.

Hasimoto, H. 1959 On the periodic fundamental solutions of the Stokes equations and their application to viscous flow past a cubic array of spheres. *J. Fluid Mech.* **5,** 317–328.

Kuwabara, S. 1959 The forces experienced by randomly distributed parallel circular cylinders or spheres in a viscous flow at small Reynolds numbers. *J. Phys. Soc. Jap.* **14,** 527–532.

Sangani, A. S. & Acrivos, A. 1982 Slow flow past periodic arrays of cylinders with application to heat transfer. *Int. J. Multiphase Flow* **8,** 193–206.

Scheidegger, A. E. 1974 *The Physics of Flow Through Porous Media*, 3rd edn. University of Toronto Press, Toronto.

Wang, C. Y. 1993 Stokes flow through a two-dimensional filter. *Phys. Fluids A* **5,** 1113–1116.

Weil, H. 1951 On the extrusion of a very viscous liquid. *J. Appl. Mech.* **18,** 267–272.

Zick, A. A. & Homsy, G. M. 1982 Stokes flow through periodic arrays of spheres. *J. Fluid Mech.* **115,** 13–26.